A&A 411, 595–604 (2003)
DOI: 10.1051/0004-6361:20031538

Astronomy & Astrophysics

Doppler imaging of stellar surface structure

XXI. The rapidly-rotating solar-type star HD 171488 = V889 Hercules

K. G. Strassmeier[1,⋆], T. Pichler[2], M. Weber[1,⋆], and T. Granzer[1]

[1] Astrophysical Institute Potsdam, An der Sternwarte 16, 14482 Potsdam, Germany
e-mail: MWeber@aip.de;TGranzer@aip.de
[2] Institut für Astronomie, Universität Wien, Türkenschanzstr. 17, 1180 Wien, Austria
e-mail: pichler@astro.univie.ac.at

Received 3 June 2003 / Accepted 9 September 2003

Abstract. We present the first Doppler image of the single G0-dwarf HD 171488. As a 30-Myr young field star with a lithium abundance of ≈140-times that of the Sun and a rotation 20 times faster, it is hardly a "solar analog" but could be termed an "infant Sun". Its position in the H-R diagram suggests it to be in the rapid-braking phase just prior to arrival on the ZAMS. Our Doppler images from four spectral lines show a cool polar spot and various high-latitude spot features with a temperature contrast of 500–1600 K relative to the effective (photospheric) temperature. Low-to-medium latitude features may be present but appear to be biased by the uneven phase coverage of our spectra and are too weak to be conclusively judged significant. We determine the rotational period to be 1.3371 ± 0.0002 days and find a long-term, possibly cyclic variation of the mean V brightness of ≈7 yrs. A constant radial velocity of -23.6 ± 1.5 km s^{-1} suggests that HD 171488 is indeed a single star. Rising flux-tube models indicate preferred surfacing latitudes between 25°–60° for HD 171488 while our Doppler images reveal mostly high-latitude spots in excess of 60°. We emphasize that this discrepancy exists for all rapidly rotating single G dwarfs observed so far.

Key words. stars: activity – starspots – stars: imaging – stars: individual: HD171488 – stars: late-type

1. Introduction

The research of magnetic activity of late-type stars and its underlying dynamo process greatly benefitted from continuous long-term studies of the behavior of surface structure such as chromospheric plages and photospheric starspots (e.g. Schrijver & Title 2001). While classical time-series photometry and spectrophotometry have the power to detect brightness variations and its periodicity, it is nevertheless limited due to its one-dimensional character. Doppler imaging, on the other hand, is a way to resolve the surface of a rotating star without actually spatially resolving the stellar disk. Reviews of this technique along with a presentation of the basic ingredients of our own Doppler-imaging code were given recently by Rice (2002) and Rice & Strassmeier (2000). Several groups in the world nowadays apply and continuously develop the numerical techniques that help to solve the ill-posed problem of Doppler imaging (e.g. Piskunov & Kochukhov 2002; Savanov 2002; Berdyugina 1998; Donati & Collier Cameron 1997). A summary of existing Doppler images of late-type stars was recently given by Strassmeier (2002).

In the present series of papers, we apply our own mapping code to spectra obtained at various observatories that maintain high-resolution spectrographs (in our case CFHT, KPNO, NSO and ESO). We follow two approaches. Firstly, we try to enlarge the astrophysical parameter space in the H-R diagram with new targets. This may eventually lead to a relation between the surface spot distribution and a rotational or stellar-structure parameter. Secondly, we try to monitor a few selected targets for decades in order to detect a cyclic behavior of the surface spot distribution, and possibly *observe* a stellar butterfly diagram. Together with a quantitative detection of differential surface rotation and meridional motion, a butterfly diagram would strongly constrain the type and mode of the dynamo process in a star's interior (e.g. Rüdiger & Elstner 2002). Further progress is expected from the coupling of the rise of magnetic flux tubes with photospheric and sub-photospheric velocity fields, which also may help to settle issues regarding the location and type of dynamo (i.e. mean field vs. shear layer and $\alpha\Omega$ vs. α^2; see e.g. Brandenburg & Dobler 2002).

Solar-twin stars would be the best targets for direct comparisons with global solar data but, unfortunately, they are –

Send offprint requests to: K. G. Strassmeier,
e-mail: KStrassmeier@aip.de

⋆ Visiting Astronomer, Kitt Peak National Observatory, operated by the Association of Universities for Research in Astronomy, Inc. under contract with the National Science Foundation.

Table 1. Observing log for our new spectra and a summary of available radial velocity measurements. Errors quoted for the KPNO, ESO, and CFHT spectra are from a Gaussian fit to the cross correlation function. HJD is 2 440 000 plus the value listed. λ denotes the central wavelength.

HJD (244+)	$v_{\rm rad}$ (km s^{-1})	λ (Å)	Source
09442.	−23.0 ± 1.2	6700	(1)
09600.	−20.6 ± 2.4	Ca K	(1)
09619.685	−22.8 ± 0.7	6430	(2)
09622.605	−22.7 ± 0.7	6430	(2)
09632.606	−11.4 ± 1.0	6170	(3)
09901.818	−21.7 ± 0.7	Hα	(2)
09903.819	−23.2 ± 0.7	6430	(2)
10221.765	−22.7 ± 1.6	6422	ESO
10222.753	−24.7 ± 1.6	6422	ESO
10225.739	−24.0 ± 1.7	6422	ESO
10226.739	−21.4 ± 2.1	6422	ESO
10906.9651	−25.1 ± 2.1	6500	KPNO
10907.9563	−24.4 ± 1.9	6500	KPNO
10908.0035	−25.8 ± 1.9	4020	(4)
10908.9772	−24.4 ± 1.9	6500	KPNO
10911.9310	−24.2 ± 1.9	6500	KPNO
10912.9409	−24.7 ± 1.9	6500	KPNO
10913.9524	−23.9 ± 1.9	6500	KPNO
10914.9768	−24.2 ± 2.0	6500	KPNO
10916.9430	−24.4 ± 1.8	6500	KPNO
10917.9440	−23.9 ± 1.9	6500	KPNO
10918.9316	−24.8 ± 1.8	6500	KPNO
10919.9822	−25.7 ± 2.0	6500	KPNO
10920.9470	−25.7 ± 2.2	6500	KPNO
10922.9625	−26.4 ± 2.0	6500	KPNO
10924.9691	−25.1 ± 2.1	6500	KPNO
10925.9598	−26.0 ± 2.2	6500	KPNO
10954.4807	−22.1 ± 1.1	6710	(5)
10957.4914	−22.7 ± 2.9	Hα	(5)
10959.4700	−25.8 ± 4.8	Ca K	(5)
11076.6513	−21.8 ± 2.4	6630	(4)
11668.8211	−22.0 ± 1.0	6430	KPNO
11669.0097	−20.0 ± 1.5	6430	KPNO
11672.0029	−22.4 ± 1.4	6430	KPNO
11672.9482	−22.4 ± 1.3	6430	KPNO
11684.1008	−23.2 ± 1.4	6710	CFHT
11684.1090	−23.3 ± 1.6	6710	CFHT
11684.1171	−23.2 ± 1.4	6710	CFHT

(1) Cutispoto et al. (2002); (2) Fekel (1997); (3) Osten & Saar (1998); (4) Strassmeier et al. (2000); (5) Cutispoto et al. (1999). KPNO, CFHT and ESO denote spectra from this paper.

so far – out of reach for the Doppler-imaging technique because of their small rotational line broadening. Only comparably very rapidly rotating stars can be mapped, but see Hatzes (1993) for numerical tests. The currently lower limit is about ten times the solar angular velocity (Strassmeier & Rice 1998; Washuettl & Strassmeier 2001). Bright, rapidly-rotating solar-type targets for Doppler imaging are therefore rare. A spectroscopic and photometric survey of 1058 late-type stars selected from a color and brightness limited subsample of the Hipparcos-Tycho catalog (cf. Vienna-KPNO H&K survey; Strassmeier et al. 2000) resulted in only one solar-like star suitable for Doppler imaging: i.e. HD 171488, G0-2V, $\alpha = 18^{\rm h}34^{\rm m}20^{\rm s}$, $\delta = +18^\circ41'24''$. In the current paper, we present its first Doppler image (Sect. 4) and determine its basic astrophysical parameters (Sect. 3). Section 5 summarizes our conclusions.

2. Observations

2.1. New spectroscopy

Moderately high-resolution spectroscopic observations were obtained with the coudé spectrograph at the coudé feed telescope of Kitt Peak National Observatory (KPNO) between April 3–22, 1998. The 3096 × 1024 F3KB CCD with 15μ pixels was used in combination with grating A, camera 5, and the long collimator. It allowed for a resolving power of 28 000 in the red-wavelength regions centered at 648.0 nm with a useful wavelength range of 30 nm. Integration time was 3600 s. Four spectra in the 643.0-nm region were obtained with the same instrumental set-up in April 2000. Four more spectra were taken earlier at ESO with the coudé auxiliary telescope in May 1996. The CES spectrograph was employed with the Loral 2688-pixel CCD at a resolving power of 70 000 and a useful wavelength range of 7 nm. Finally, a set of three spectra of the lithium region was obtained with the Gecko spectrograph on the 3.6-m CFH-telescope (CFHT). The resolving power was 120 000, and the useful wavelength range was 10 nm with the 4400-pixel EEV1V CCD. All spectra have signal-to-noise ratios in excess of 200:1. Table 1 is a summary of the spectroscopic observations (marked as KPNO, ESO and CFHT) together with a listing of previously published radial velocities. Note that only the April-1998 KPNO data (JD 2 440 906–925) are used for Doppler imaging.

Figure 1 displays a typical single-exposure spectrum of HD 171488 from the KPNO run in April 1998. The reduction procedure was identical to that in recent papers based on KPNO data, e.g. Weber & Strassmeier (2001), obtained with the same instrumental set up and we refer the reader to that as well as to previous papers in this series. Spectra from ESO and CFHT were treated similarly as described in Rice & Strassmeier (2001). At KPNO, a radial-velocity standard was observed at the beginning (β Gem) and at the end of each night (16 Vir) and provided the absolute zero point of our radial-velocity calibration. ζ Oph was used as a telluric calibration star.

2.2. Time-series photometry

Continuous photometric observations were obtained with Wolfgang and Amadeus, the two 0.75-m Vienna-Observatory Automatic Photoelectric Telescopes (APT) at Fairborn Observatory (Strassmeier et al. 1997). The observations started in 1996/97 with a sampling of one to three points per night and are still being continued. Data prior to 1997/98 were published by Strassmeier et al. (1999). A total of 1095 VI and 384

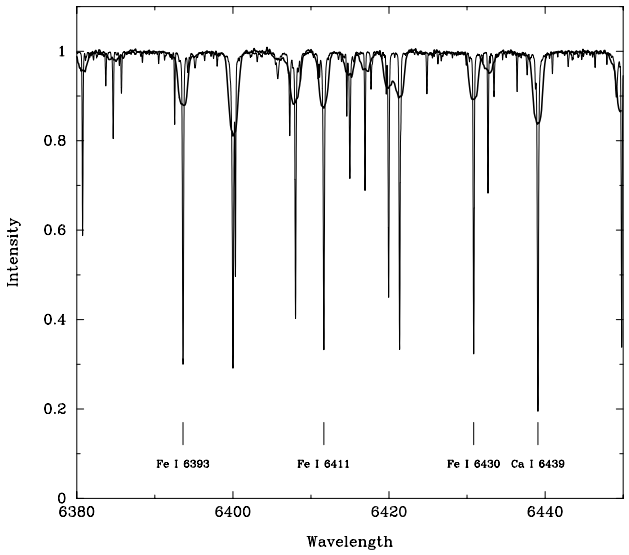

Fig. 1. An example spectrum of HD 171488 (thick line). For comparison purposes, a very high-resolution spectrum of the Sun is also shown (thin line). The four spectral lines adopted for Doppler imaging are marked.

by measurements, each the mean of three 10-s readings per filter with an internal standard deviation of less than 5 mmag, constituted the useable data set for this paper. Measurements with a larger internal standard deviation were discarded. A diaphragm of 30″ was used for all integrations.

All data were taken in and transformed to either the Johnson-Cousins *VRI* system or the Strömgren *uvby* system and used HD 171286 (K0V, $V = 6\overset{\mathrm{m}}{.}835$, ESA 1997) and HD 170829 (G8IV) as the comparison and check star, respectively. For the data reduction procedure we refer to Strassmeier et al. (2000, 1999).

3. Astrophysical parameters of HD 171488

3.1. Magnetic activity

HD 171488 was detected with the ROSAT EUV wide field camera (Pounds et al. 1993) and is listed in the 2RE source catalog as 2RE J183421+184114 with a count rate of 0.033 ct s^{-1} (Pye et al. 1995). As far as we know no pointed observations were made with ROSAT or XMM-Newton and Chandra. The star was detected by the Extreme Ultra-Violet Explorer in its 100-Å all-sky survey with 0.043 ct s^{-1} (Bowyer et al. 1996). The count rates suggest that HD 171488 possesses an active corona.

Mulliss & Bopp (1994) found weak Hα and Ca II 854.2nm absorption lines, indicating an active chromosphere. The star also exhibits strong Ca II H&K emission with absolute emission line fluxes of 6×10^6 erg cm^{-2} s^{-1}, i.e. 1.4×10^{-4} in units of the bolometric luminosity (Strassmeier et al. 2000). These are values slightly smaller but comparable to the most active stars known to date. Hα was verified as a filled-in absorption profile.

3.2. Radial velocities

Radial velocities for our KPNO spectra were derived from cross correlations with spectra of IAU velocity standards (as described in more detail in Fekel et al. 1999). All cross correlations were carried out with the `fxcor` routine in IRAF[1]. Its internal errors usually depend on the wavelength range covered and on the rotational broadening of the target, but also on any spectral-type mismatch between target and reference star. The external errors usually depend on the time span between the observation of the target and the reference star and whether there was some second-order drift in between (to first order this is removed by the Th-Ar calibration). However, in case of very active stars such as HD 171488 it is the line asymmetry due to spots that limits the radial-velocity accuracy. We may expect a velocity shift of the line centroid due to spots of up to a few km s^{-1} (e.g. Hatzes et al. 2002).

Table 1 lists the new velocities along with previously published ones from five additional sources. With the exception of the one measure by Osten & Saar (1998) that seems to be in error, and the two more uncertain velocities from the Ca II H&K region, the grand average is -23.6 ± 1.5 km s^{-1} (rms). A period search did result in no significant periodicity with an amplitude exceeding the rms of the mean value. Because furthermore, the rms-scatter around the mean is comparable to the error of a single measurement, we consider the radial velocity to be constant and conclude that HD 171488 is a single star.

3.3. Refinement of the rotational period

Starspots on the surface of a rotating star are like markers for the determination of its rotational period. The photometric period can thus be directly interpreted as the stellar rotation period. For the present study, we have available a much longer time baseline for a frequency analysis than before, altogether six years. We emphasize that uncertainties of the period will lead to additional uncertainties of the stellar surface map – motivation enough to redetermine the period.

Henry et al. (1995), Cutispoto et al. (1998) and Strassmeier et al. (1999) already presented photometry of HD 171488 and found its light variations with a period of approximately 1.34 days. Such a short period is in agreement with the G0 dwarf classification by Harlan (1969) based on Hγ spectra as well as the rotational velocity of 38 km s^{-1} measured by Fekel (1997). An alternative period of 1.49585 days from *Hipparcos* photometry was recently presented by Koen & Eyer (2002). This period has no counterpart in any of the ground-based data sets and we consider it spurious due to some spacecraft-related periodicity (see, e.g. Kallinger & Weiss 2002).

We first carried out a Fourier analysis of all our APT *VI* and *by* data separately and per observational season but then proceeded with the combined *V* and *y* data from all seasons (the *y* magnitudes were transformed to *V* using the relation in

[1] Image Reduction and Analysis Facility distributed by NOAO/KPNO.

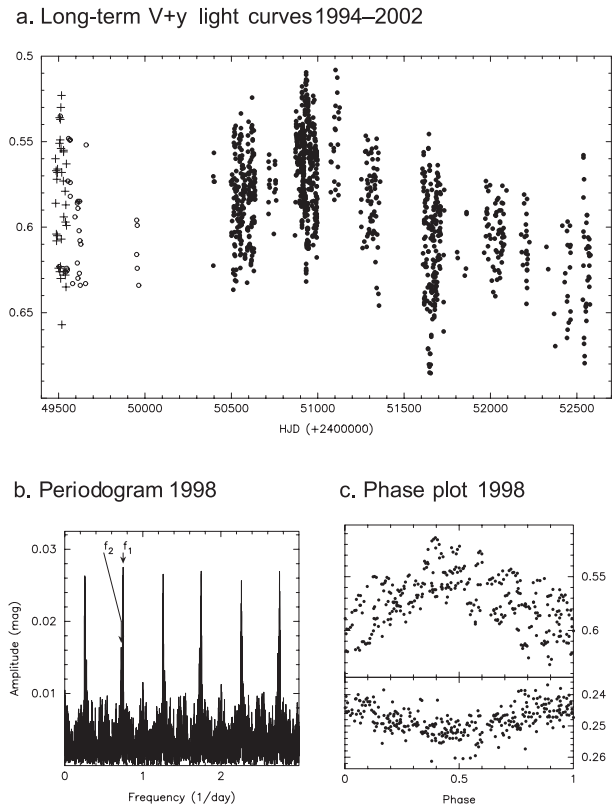

Fig. 2. a) Long-term (differential) photometry of HD 171488. Dots are our APT observations, plusses are from Henry et al. (1995), circles from Rodonó et al. (priv. commun.). **b)** Periodogram from the 1998 *by* data, and **c)** phased 1998 differential y (top) and $b-y$ (bottom) light curve with $P = 1.3371$ days (denoted as f_1 in the periodogram). See text for the explanation of f_2.

Olsen 1994). A total of 1479 new APT measures spread over 6 yrs (1095 in *VI*, 384 in *by*) plus 26 data points from the Catania APT (Rodonó et al., priv. commun.), 5 data points from ESO (Cutispoto et al. 1999) and 35 *BV* data points from Henry et al. (1995) were then available for the analysis. Before we continued with a search for the rotational period, a sinusoidal long-term trend with a possible period of 2600 ± 300 days was removed from the data. We interpret this 7-yr period to be an analog of the Sun's 11-yr sunspot cycle, in agreement with independent observations from Henry (2002, priv. commun.).

Figure 2a plots the long-term *V*-light curve from 1994–2002. Dots mark our APT data from 1997–2002, the earlier data from ESO (Cutispoto et al. 1999) and from the Catania APT (Rodonó et al., priv. commun.), and the data presented by Henry et al. (1995) are also included. Figures 2b and 2c show the resulting periodogram for the 1998 observing season and its phased light curve, respectively. The originally detected period of 1.337 days (designated f_1) is the strongest peak in each season except for maybe 1997 where its $1-f_1$ alias ($P = 3.9668$ days in 1998) is equally strong (to within a fraction of a percent).

1998 was a particularly well-sampled observing season with high-precision Strömgren data. It is used to refine the frequency values of the highest short-period peaks. A period of 1.3371 ± 0.0002 days shows the strongest reduction of

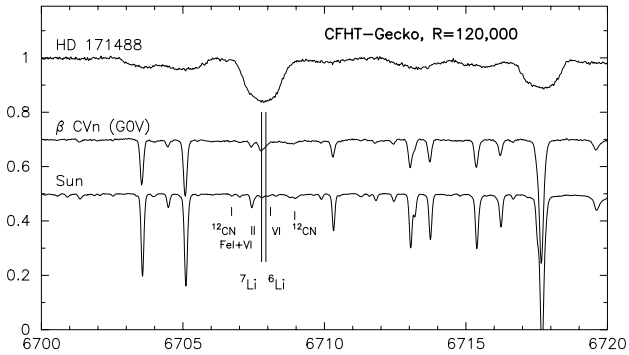

Fig. 3. Li I 670.8 nm spectrum of HD 171488. Shown are also spectra of the Sun (bottom) and β CVn (middle) for comparison purpose (both spectra are shifted). The equivalent width of the lithium line of HD 171488 is measured to be 213 ± 7 mÅ.

the residuals in 1998 (Table 3, Fig. 2). A second period very close to the main period at 1.38 days appears persistently in all seasons and could be due to a periodic change of surface spottedness, e.g. a latitudinal flip of activity coupled with differential surface rotation[2]. A third period (f_3 in Table 3) appears but is much weaker and constitutes a close triplet with f_1 and f_2. Together with the main period, f_2 produces a beat period of ≈40 days, that is easily recognizable in the Julian-date plots due to our strictly nightly observations. We conclude that 1.3371 days is the true photometric period and interpret it to be the rotational period of HD 171488.

3.4. Lithium abundance

Figure 3 shows a representative spectrum of the exceptionally strong Li I 670.8-nm line of HD 171488. Its equivalent width is 213 ± 7 mÅ as compared to 160 mÅ for the nearby Ca I 671.7nm line. The uncertainty of just 7 mÅ is estimated from different types of fits to the line profile, e.g. with a Gaussian profile of variable width where only the profile points of the red profile wing are used for the least-squares fit, from a normal Gaussian fit or from a simple profile-area integration. For the G0V star β CVn, the ^{12}CN and Fe blend in the blue wing of the Li line (see Fig. 3) amount to 5 and 12 mÅ, respectively. Our Li equivalent width for HD 171488 is corrected for this but is still the sum from the two isotopes ^{6}Li and ^{7}Li that remain unresolved in our spectra. Earlier Li measurements of HD 171488 gave 210 ± 50 mÅ (Mulliss & Bopp 1994), 176 ± 20 mÅ (Strassmeier et al. 2000), and 220 ± 10 mÅ (Cutispoto et al. 2002). The non-LTE curves of growth of Pavlenko & Magazzú (1996) for a 5800 K/$\log g = 4.5$ model convert an equivalent width of 213 mÅ of a G0 dwarf into a Li abundance of 3.3 ± 0.1 (on the $\log n(\mathrm{H}) = 12.00$ scale). On this scale the observed solar photospheric Li abundance listed by Grevesse & Sauval (1998) is 1.16 ± 0.1, and the Li-670.8 line appears to have an equivalent width of around 2 mÅ. The large Li abundance of HD 171488 is close to the primordial

[2] In case a light curve would be double-humped throughout the observations, e.g. when two active longitudes separated by 180° persistently exist, a frequency f from a sine-curve fit would result in a rotation period of $2/f$, i.e. 2.67 days for f_1 instead of 1.337 days.

value usually only seen in pre-main-sequence stars but would be consistent with a lithium depletion isochrone by Chaboyer et al. (1995) of age ≈50 Myrs. For comparison, the average equivalent width of the three G0 stars in the 30-Myr young open cluster IC 2602 is 188 mÅ (Randich et al. 1997), while the corresponding value in the ≈100-Myr old Pleiades is near 130 mÅ (Soderblom et al. 1993).

3.5. Rotational line broadening and the inclination of the rotational axis

Henry et al. (1995) first quoted a $v \sin i$ value of 33 km s^{-1} that was later revised by Fekel (1997) to 38.0 km s^{-1} based on high-resolution red-wavelength spectra. This value was confirmed by Osten & Saar (1998) from even higher resolution echelle data. Cutispoto et al. (1999) obtained a value of 40 ± 2 km s^{-1} from ESO spectra while Strassmeier et al. (2000) obtained 36 ± 2 km s^{-1} from a single moderate-resolution spectrum. Recently, Cutispoto et al. (2002) listed a value of 45 km s^{-1} from CORAVEL data but gave no error bar. Note that $v \sin i$ is later refined in the Doppler-imaging process in this paper to 39.0 ± 0.5 km s^{-1}, which is the value adopted in this paper (see Sect. 4).

With the observed rotational velocity of 39 km s^{-1} and the rotation period P of 1.3371 days, the minimum radius is 1.03 ± 0.01 $R_\odot$. Together with the luminosity from the parallax, we can estimate the inclination of the stellar rotation axis from the difference of $R \sin i$ to the nominal radius of a G0V star. The Landolt-Börnstein tables (Schmidt-Kaler 1982) list a radius for a G0V star of 1.10 $R_\odot$. If adopted for HD 171488, an inclination near 69° is expected.

An inclination of below ≈15° is unlikely because we detect fairly large rotational modulations with a full amplitude of $0\overset{\mathrm{m}}{.}15$ in V in e.g. 2000. In spite that simple numerical simulations (e.g. Strassmeier 1996) show that an amplitude of $0\overset{\mathrm{m}}{.}15$ can be obtained even at an inclination of as low as 15° in case a single black spot as large as a hemisphere exists, the then expected line profiles are not supported by our observations. We therefore adopted an initial inclination of 65° for the first round of Doppler imaging but refine that value to 55° in Sect. 4.2.

3.6. Absolute dimensions and age

The parallax from *Hipparcos* (ESA 1997) confined the distance of HD 171488 to 37.2 ± 1.2 pc. If we adopt the maximum visual brightness of $V = 7\overset{\mathrm{m}}{.}34$ observed in 1998 (Fig. 3)[3], and negligible interstellar absorption, the absolute visual brightness is $M_V = +4.49 \pm 0.07$ mag. Adopting a bolometric correction of −0.070 from Flower (1996) based on $T_{\rm eff} = 5830$ K from $B-V$, the luminosity is 1.33 ± 0.09 $L_\odot$ (with $M_{\rm bol,\odot} = +4\overset{\mathrm{m}}{.}73$). The stellar radius is thereby confined to 1.09 ± 0.05 $R_\odot$ due to the errors of $\pm 0\overset{\mathrm{m}}{.}07$ in $M_{\rm bol}$ and ±50 K in $T_{\rm eff}$, thus in good agreement with the G0V spectrum classification.

[3] We note that Perry (1969) listed a single Strömgren measurement of $7\overset{\mathrm{m}}{.}30$ and $b-y = 0.408$ which indicates that HD 171488 may have had an even brighter maximum in the past. Olsen (1994) listed $7\overset{\mathrm{m}}{.}456$ and $b-y = 0.413$ for 1988–91 and Olsen (1983) listed $7\overset{\mathrm{m}}{.}389$ for 1978, while the average Hipparcos-Tycho entry is $7\overset{\mathrm{m}}{.}39$ for 1991 (Koen & Eyer 2002).

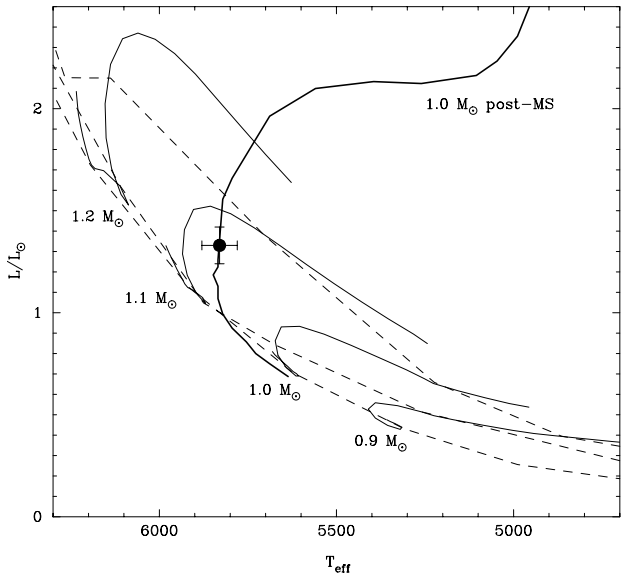

Fig. 4. The position of HD 171488 in the H-R diagram. The thin lines are the pre-main-sequence tracks of D'Antona & Mazzitelli (1997) for masses of 0.9, 1.0, 1.1, and 1.2 solar masses. The dotted lines are three isochrones for ages of 20, 30, and 100 Myrs (from top to bottom). The thick full line is a single post-main-sequence track for 1.0 solar mass from Schaller et al. (1992). The tracks suggest a (pre-main-sequence) mass of around 1.06 $M_\odot$.

Figure 4 shows the position in the H-R diagram with respect to current evolutionary tracks. The lines are the pre-main-sequence tracks from D'Antona & Mazzitelli (1997) for 0.9–1.2 $M_\odot$, and the thick line is a post-main-sequence track of one solar mass from Schaller et al. (1992). The dotted lines are isochrones for 20, 30, and 100 Myrs, respectively. The star is very close but not yet on the theoretical ZAMS at an age of close to 30 Myrs, in agreement with its high lithium abundance, and may be in the middle of its rapid-braking phase (cf. Charbonneau & MacGregor 1992). A straightforward interpolation within the D'Antona & Mazzitelli tracks suggests a mass of around 1.06 $M_\odot$.

Table 2 summarizes the properties of HD 171488.

4. A Doppler image for April 1998

4.1. Basic TempMap-code parameters

Our Doppler imaging program (TEMPMAP) is in continuous development based on the original code by Rice et al. (1989). It inverts spectral-line profiles into a surface temperature distribution with the help of a penalty function and based on numerically tabulated local line profiles from a grid of model atmospheres and a radiative-transfer computation at many aspect angles. An updated description is given by Rice (2002). Extensive numerical tests were presented in Rice & Strassmeier (2000) and Strassmeier et al. (2003). For details, we refer the reader to these and to previous papers in this series.

Table 2. Stellar parameters of HD 171488.

Parameter	Value
Distance (Hipparcos)	37.2 ± 1.2 pc
Spectral type	G0V
$V_{\rm max}$	$7\overset{\rm m}{.}34$
M_V	4.49 ± 0.07 mag
Luminosity	1.33 ± 0.09 $L_\odot$
$T_{\rm eff}$	5830 ± 50 K
Mass	1.06 ± 0.02 $M_\odot$
Radius	1.09 ± 0.05 $R_\odot$
Period	1.3371 ± 0.0002 days
$v \sin i$	39.0 ± 0.5 km s^{-1}
Inclination	≈55°
Microturbulence	1.0 km s^{-1}
Macroturbulence $\zeta_{\rm R} = \zeta_{\rm T}$	3.0 km s^{-1}
Fe/Fe$_\odot$	–0.5
Ca/Ca$_\odot$	–0.35
Li/Li$_\odot$	+2.14

Table 3. Summary of photometric periods and aliases in days for the 1998 Strömgren data set. The significance of a period is indicated by its amplitude in the b and y bandpasses and the resulting signal-to-noise ratio (S/N) in y.

Freq. peak	P (days)	Δy (mmag)	Δb (mmag)	S/N (y)
f_1	1.33706 ± 0.00024	28.5	28.3	6.2
f_2	1.3807 ± 0.0033	15.0	19.0	4.8
f_3	1.3594 ± 0.025	13.5	8.8	4.1
1-f_1	3.9669 ± 0.0021	22	22	5.6

4.2. Adopted input parameters

As in our previous papers, the radiative transfer calculations are based on ten plane-parallel LTE model atmospheres with temperatures from 3500 K to 6500 K taken from the ATLAS-9 grid (Kurucz 1993). A gravity of $\log g = 4.5$, a microturbulence of 1 km s^{-1}, and a macroturbulence of 3 km s^{-1} were adopted from Gray (1992) and Fekel (1997), respectively, based on a ≈G0V spectral classification. We emphasize that we found no significant differences to local profiles from ATLAS-12 atmospheres that were computed with the Canuto & Mazzitelli (1992)-treatment of convective flux (cf. Kupka 1996; Strassmeier & Rice 1998). Further stellar input parameters of HD 171488 are listed in Table 2.

The final values for $v \sin i$ and the inclination i were obtained with TempMap by iteratively changing one parameter at a time. The $v \sin i$ range was limited to 32–45 km s^{-1} (the literature values plus/minus 1 km s^{-1}) and the inclination to 10–80°. The best fits were obtained for $v \sin i = 39.0$ km s^{-1} (Fig. 5) and $i = 55°$.

The atomic data for the mapping lines and their blends were generally taken from VALD (Vienna Atomic Line Database; Kupka et al. 1999) with some exceptions found and tabulated

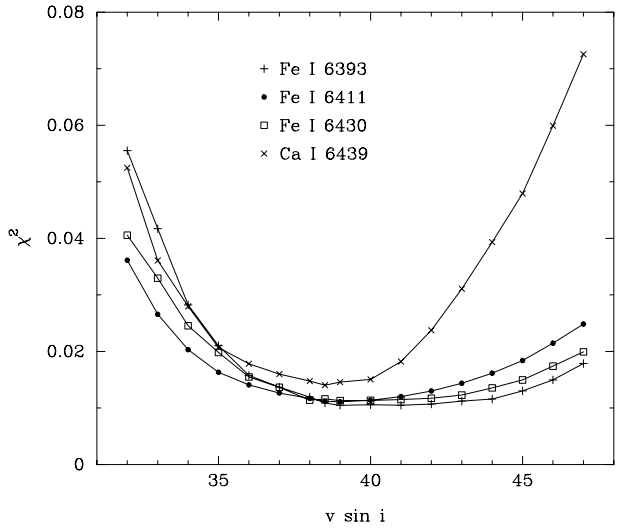

Fig. 5. The misfit (χ^2) between the observed and the computed line profiles as a function of rotational broadening ($v \sin i$). The value with the smallest residuals is 39.0 ± 0.5 km s^{-1} at an inclination of ≈55°.

in previous papers in this series (e.g. in Strassmeier & Rice 2003 for the G0V primary of σ^2 CrB). Abundances were initially kept at the solar value by default but the Fe and Ca abundance were adjusted during the imaging. This is possible with TempMap because a general underestimation of the line equivalent width must be either compensated with easily recognizable artificial bright regions, preferably at circumpolar latitudes (see, e.g. Kratzwald 2003 or Strassmeier et al. 2003), or by a change of the elemental abundance and/or the intrinsic line strength ($\log gf$). The latter is well determined from laboratory measurements and thus the bright regions can only be minimized by varying the abundance. The values that gave the best compromise were 7.13 for Fe and 5.97 for Ca (on the regular $\log n(\rm H) = 12.00$ scale). Both values indicate an underabundance of these two elements relative to the solar photosphere of 0.5 dex for Fe and 0.35 dex for Ca. A comparison of Doppler maps of HD 171488 computed with formal solar abundances was given in Pichler (2002) and resulted in a higher average surface temperature by 500 K but otherwise identical surface morphology. As in previous papers (see again Strassmeier & Rice 2003 and references therein), we estimate the external uncertainty to be ±0.1 dex and therefore consider the underabundance to be a real effect.

4.3. Surface maps

Figure 6 shows the Doppler images of HD 171488 derived with a rotation period of 1.337 days from Ca I 643.9 nm, Fe I 643.0 nm, Fe I 641.1 nm and Fe I 639.3 nm. Figure 7a shows the average map from these four lines and Fig. 7b the corresponding standard-deviation map. As in previous papers in this series we chose equal weights for the averaging of the individual lines because *i)* the overall fitting errors are comparable and, *ii)*, the formation heights in the stellar photosphere are also comparable, i.e. that these lines should be affected by the same spot distribution (under the assumption of solar analogy). A weighting with the inverse of the overall fitting error, as

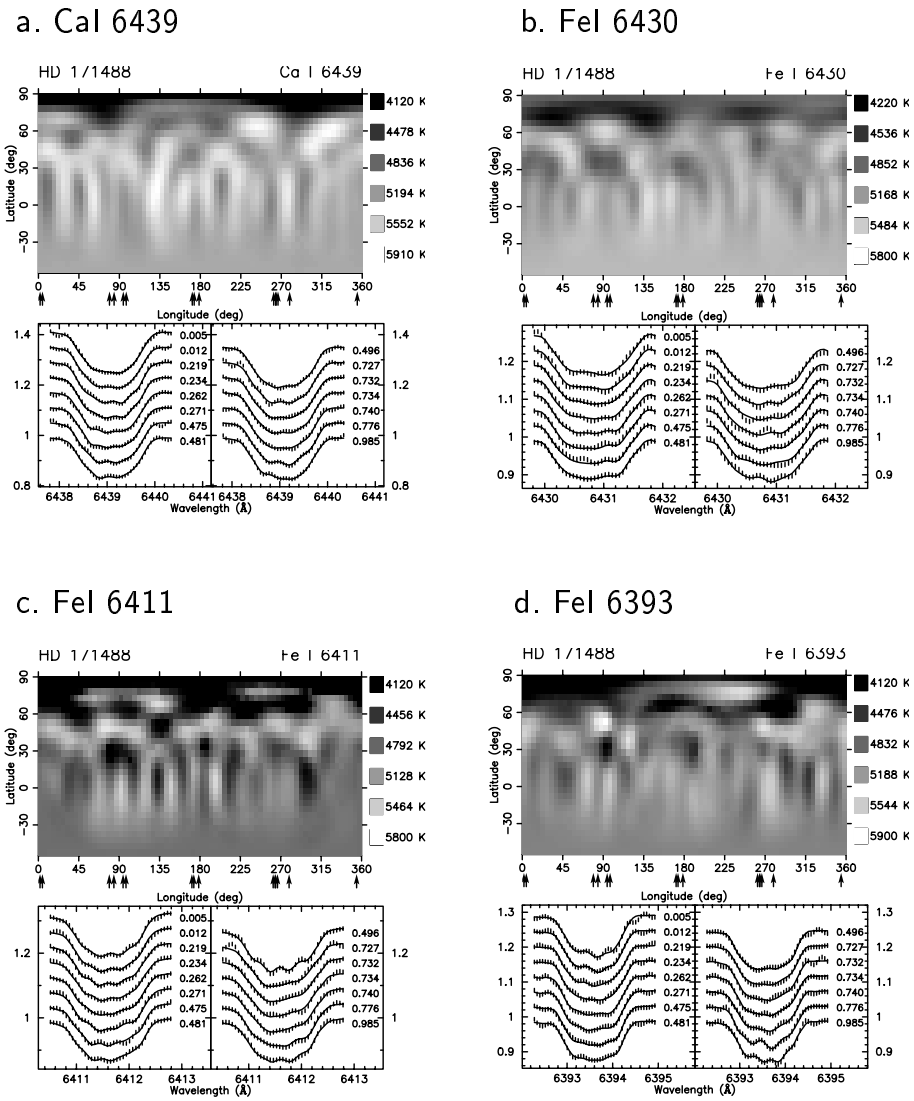

Fig. 6. Doppler images (top) and line-profile fits (bottom) from four spectral lines. **a)** Ca I 643.9 nm, **b)** Fe I 643.0 nm, **c)** Fe I 641.1 nm, and **d)** Fe I 639.3 nm. The arrows below each map indicate the phase coverage of the spectra.

pointed out by the referee as another possibility, would change a pixel's temperature by less than 10 K (≤0.01%) as compared to the unweighted average. The simple averaging has the advantage that not only consistent surface features appear emphasized while others will be suppressed but also that imperfect blend removal from one line region to the other, which could also lead to an artificially overall better fit for a particular line region, will be averaged out. Unless we are not 100% sure about the atomic blends and their parameters, the unweighted average map represents our best and simplest reconstruction of the surface of HD 171488 from the given data. An asymmetric polar spot with $\Delta T \approx 1600$ K dominates the maps. Its appendages reach lower latitudes of around 60°. Several lower-contrast spots with $\Delta T \approx 500$–800 K appear at low latitudes but their detection is comparably more uncertain due to the non-uniform phase coverage (due to the rotation period of 1.34 days, which beats at $1 - f \approx 4.0$ days).

The quality of the data and its fits is also shown in Fig. 6. The respective lower panels show the observed line-profile data as bars and the fits as continuous lines. The length of a bar marks $\pm 1\sigma$. Note that TempMap not only fits the line profiles and the b and y light-curve shape simultaneously, but also the $b - y$ index (see Rice 2002).

The maps were obtained with a maximum-entropy regularization set to a smoothing factor of 5.0 and a maximum of 15 iterations (see Rice & Strassmeier 2000; Strassmeier et al. 2003). These numbers are appropriate for the S/N of the KPNO spectra of around 200:1. Photometry was not included. Maps with photometric input were also computed but because the photometric coverage during the 19 days of spectroscopic observations was comparably sparse (see Pichler 2002), we adopted the maps without photometry as our standard. The inclusion of photometry just smears the temperature gradients but the maps appear otherwise identical. Fitting errors were for Ca I 643.9 nm 1.404×10^{-2}, for Fe I 643.0 nm 1.160×10^{-2}, for Fe I 641.1 nm 1.117×10^{-2} and for Fe I 639.3 nm 1.087×10^{-2}. Error is defined here as $\sqrt{\sum(\mathrm{O} - -\mathrm{C})^2/(N-1)}$ where N is the total number of spectrum points in all of the observations,

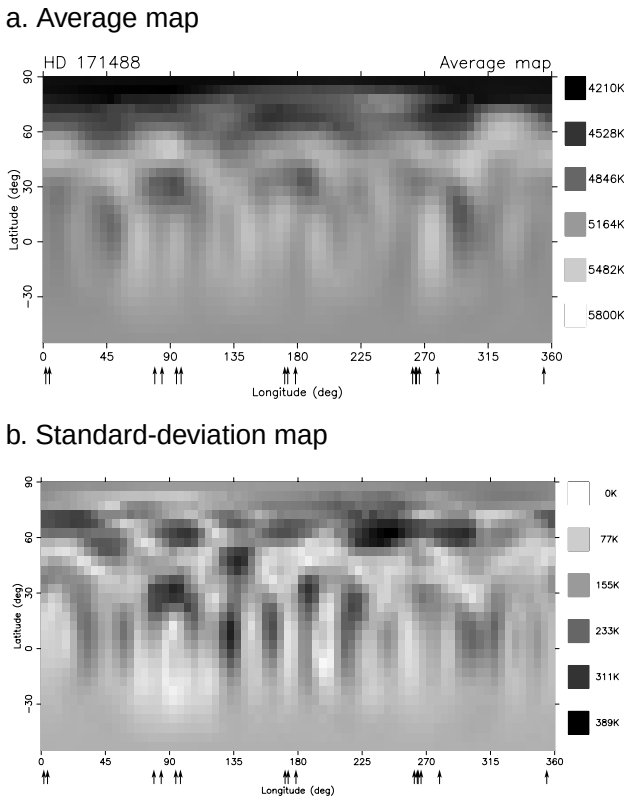

Fig. 7. a) Average and **b)** standard-deviation maps from the four single-line inversions in Fig. 6. We consider the average map to be the most reliable map from our current data set.

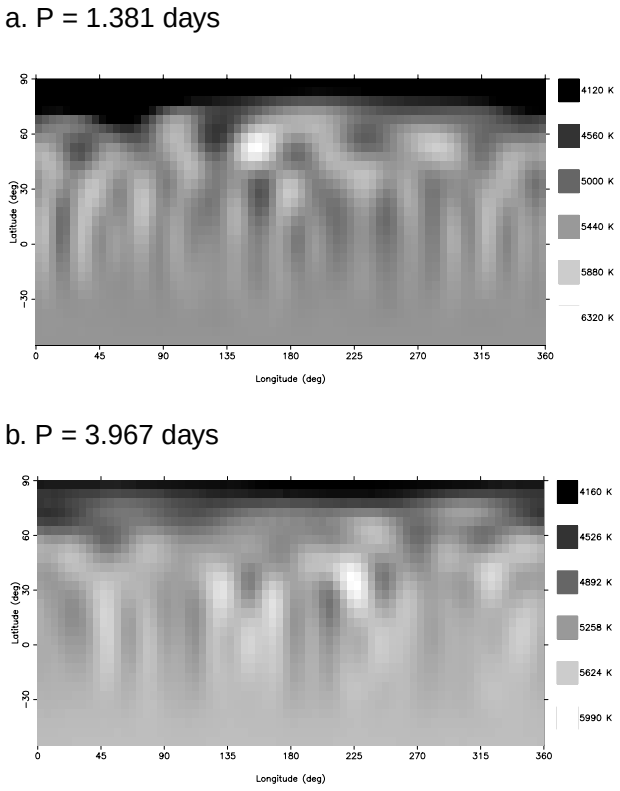

Fig. 8. Example Doppler maps from Ca I 643.9 nm for rotational periods of **a)** 1.381 days (f_2) and **b)** 3.967 days ($1 - f_1$). These maps are to be compared with the preferred $P = 1.337$-days map in Fig. 6a or the average map in Fig. 7a.

i.e. the number of pixels per phase times the number of phases. In case there is also photometric input its O–C's squared are added with a weight of 0.1.

Before we interpret the maps we recall that the period search in Sect. 3.3 suggested three possible photometric periods with almost equally reduced residuals for the two photometric bandpasses, i.e. 0.572 days ($=1+f_1$), 1.337 days ($=f_1$), 1.381 days ($=f_2$), and 3.967 days ($=1-f_1$) (see Fig. 2b and Table 3). Two of them are aliases of the true 1.337-day rotation period while the f_2 period is part of a close triplet ($f_1\, f_2\, f_3$) with f_1 as the main peak. Therefore, we computed Doppler maps by using the alias periods as well as the close f_2 period and compared them with the map from f_1.

Once $v \sin i$ is fixed to 39 km s^{-1} and $R = 1.09\ R_\odot$ (cf. Sect. 3.6) the inclination of the rotational axis for the $1+f_1$ and f_2 periods (cf. Table 3) is 24° and 78°, respectively, while the 3.967-day period results in $\sin i > 1$, or a sub-giant classification rather than a dwarf, which would be in contradiction with the optical spectra and the Hipparcos parallax. Therefore, we may already exclude the 3.967-day period on that ground. The existence of the close 1.381-day period ($=f_2$) may be an indicator that part of the power seen in the 1.337-day period is spurious. At least there is a slight chance that the true stellar rotation period is just near the value that we used for computing our maps. Therefore, we formally regard our maps as preliminary.

Figures 8a and 8b show the Ca-maps for rotational periods of 1.381 days and 3.967 days, respectively. These maps are to be compared with the 1.337-day maps in Figs. 7a and 6a. The fitting errors with $P = 3.967$ are for all lines 5–10% worse than for the 1.337-day period, while the fits with $P = 1.381$ are better by almost 10% for Ca I 643.9 and Fe I 643.0 but worse by a few per cent for the other two lines. As shown in Fig. 8a, the surface spot morphology for $P = 1.381$ days becomes increasingly detailed at low latitudes while, at the same time, some of the major bumps in the profiles are not fitted as nice as in case of the 1.337-day period. Obviously, comparably small changes of the overall χ^2 are not always an acceptable indicator for the detection of "false" maps and we still conclude that the maps with 1.337 days are most likely the true ones.

5. Summary and conclusions

HD 171488 is a rapidly-rotating single G0 star at an age of approximately 30–50 Myrs. Its exceptionally high lithium abundance of close to the primordial value is in good agreement with the young age from a comparison with pre-main-sequence isochrones from D'Antona & Mazzitelli (1997) and the lithium depletion isochrones from Chaboyer et al. (1995). HD 171488 is thus among a group of very young rapidly rotating single stars just approaching the main sequence. Table 4 lists other such stars, all of them with published Doppler maps. A comparison shows that all of them exhibit high-latitude spot activity and, with one exception (AP 193), also have a "polar spot". Theoretical models of flux-tube emergence (cf. Granzer 2002) predict only low-to-moderate latitude spot emergence for all of

Table 4. Single G-type stars with Doppler images.

MK-class	Star name	Age (Myr)	P_{rot} (days)	Spots observed[d]	Ref.	Spots predicted[e]
G0V	HD171488	30–50	1.337	PH(L)	(1)	25–60
G1.5V	EK Dra	120	2.605	PHL	(2)	20–60
G1-2V	HII 314	100[a]	1.470	PHL	(3)	20–60
G2V-IV	RXJ1508.6	25[b]	0.310	PHL	(4)	35–60
G2-3V	He 699	50–70[c]	0.491	PH	(5, 6)	30–60
G5-6V	AP 193	50–70[c]	0.748	H	(5)	25–60
G6V	He 520	50–70[c]	0.604	PHL	(5)	25–60
G8V	AP 149	50–70[c]	0.320	PH	(5)	35–60

[a]Pleiades, [b]Lupus SFR, age ± 10 Myr, [c]α Per stars. [d] P = Polar spot, H = High-latitude spots, L = Low-latitude spots. [e]Latitude range of highest spot probability in degrees from rising flux-tube models (cf. Granzer 2002; Granzer et al. 2000).
(1) This paper; (2) Strassmeier & Rice (1998); (3) Rice & Strassmeier (2001); (4) Donati et al. (2000); (5) Barnes et al. (2001); (6) Jeffers et al. (2002).

them. It seems clear now that our current theoretical explanation for the existence of starspots is not complete as previously suggested by several authors (see, e.g., the review by Schrijver 2002).

One of the next steps in the papers of this series will involve the search for systematic migration patterns from well-sampled spectroscopic time series over periods of several months. From this we hope to extract information on meridional-circulation velocities.

Acknowledgements. K.G.S. is very grateful to the German Science Foundation (DFG) for support under grant STR645/1. We thank P. Reegen, Vienna, for his help with the period analysis and APT data reduction. Thanks are also due to G. Cutispoto et al., Catania, for allowing us to use part of the Catania-APT data prior to publication and to G. Henry, TSU-Nashville, for making his previously published data available to us.

References

Barnes, J. R., Collier Cameron, A., James, D. J., et al. 2001, MNRAS, 326, 1057
Berdyugina, S. V. 1998, A&A, 338, 97
Bowyer, S., Lampton, M., Lewis, J., et al. 1996, ApJS, 102, 129
Brandenburg, A., & Dobler, W. 2002, AN, 323, 411
Breger, M. 1990, Comm. in Asteroseism., 1
Canuto, V. M., & Mazzitelli, I. 1992, ApJ, 389, 724
Charbonneau, P., & MacGregor, K. B. 1992, ApJ, 397, L63
Chaboyer, B., Demarque, P., & Pinsonneault, M. H. 1995, ApJ, 441, 876
Cutispoto, G., Tagliaferri, G., Kürster, M., Messina, S., & Rodonó, M. 1998, in Cool Stars, Stellar Systems, and the Sun, ed. R. A. Donahue, & J. Bookbinder, PASPC 154, CD1397
Cutispoto, G., Pastori, L., Tagliaferri, G., Messina, S., & Rodonó, M. 1999, A&AS, 138, 87
Cutispoto, G., Pastori, L., Pasquini, L., et al. 2002, A&A, 384, 491
D'Antona, F., & Mazzitelli, I. 1997, in Cool stars in clusters and associations, ed. R. Pallavicini, & G. Micela, Mem. S. A. It., 68, 807
Donati, J.-F., & Collier Cameron, A. 1997, MNRAS, 291, 1
Donati, J-F., Mengel, M., & Carter, B. D. 2000, MNRAS, 316, 699
ESA 1997, The Hipparcos and Tycho catalog, ESA SP-1200
Granzer, T. 2002, AN, 323, 395
Granzer, T., Schüssler, M., Caligari, P., & Strassmeier, K. G. 2000, A&A, 355, 1087
Gray, D. F. 1992, The observation and analysis of stellar photospheres (Cambridge Univ. Press), 416
Grevesse, N., & Sauval, A. J. 1998, Space Sci. Rev., 85, 161
Fekel, F. C. 1997, PASP, 109, 514
Fekel, F. C., Strassmeier, K. G., Washuettl, A., & Weber, M. 1999, A&AS, 137, 369
Flower, P. J. 1996, ApJ, 469, 355
Harlan, E. A. 1969, AJ, 74, 916
Hatzes, A. P. 1993, ApJ, 410, 777
Hatzes, A. P. 2002, AN, 323, 392
Henry, G. W., Fekel, F. C., & Hall, D. S. 1995, AJ, 110, 2926
Jeffers, S. V., Barnes, J. R., & Collier Cameron, A. 2002, MNRAS, 331, 666
Kallinger, T., & Weiss, W. W. 2002, A&A, 385, 533
Koen, C., & Eyer, L. 2002, MNRAS, 331, 45
Kratzwald, L. 2003, Masters Thesis, University of Vienna
Kupka, F. 1996, in Stellar Surface Structure, ed. K. G. Strassmeier, & J. L. Linsky (Kluwer, Dordrecht), IAU Symp., 176, 557
Kupka, F., Piskunov, N. E., Ryabchikova, T. A., Stempels, H. C., & Weiss, W. W. 1999, A&AS, 138, 119
Kurucz, R. L. 1993, ATLAS-9, CD-ROM #13
Mulliss, C. L., & Bopp, B. W. 1994, PASP, 106, 822
Olsen, E. H. 1983, A&AS, 54, 55
Olsen, E. H. 1994, A&AS, 106, 257
Osten, R. A., & Saar, S. H. 1998, MNRAS, 295, 257
Pavlenko, Ya. V., & Magazzú, A. 1996, A&A, 311, 961
Perry, C. L. 1969, AJ, 74, 705
Pounds, K. A., Allan, D. J., Barber, C., et al. 1993, MNRAS, 260, 77
Pichler, T. 2002, Masters Thesis, Univ. of Vienna
Piskunov, N. E., & Kochukhov, O. 2002, A&A, 381, 736
Pye, J. P., McGale, P. A., Allan, D. J., et al. 1995, MNRAS, 274, 1165
Randich, S., Aharpour, N., Pallavicini, R., Prosser, C. F., & Stauffer, J. R. 1997, A&A, 323, 86
Rice, J. B. 2002, AN, 323, 220
Rice, J. B., & Strassmeier, K. G. 2000, A&AS, 147, 151
Rice, J. B., & Strassmeier, K. G. 2001, A&A, 377, 264 (Paper XVII)

Rice, J. B., Wehlau, W. H., & Khokhlova, V. L. 1989, A&A, 208, 179
Rüdiger, G., & Elstner, D. 2002, AN, 323, 432
Savanov, I. 2002, in Poster proceedings 1st Potsdam Thinkshop, Sunspots & Starspots, ed. K. G. Strassmeier, & A. Washuettl, AIP, 3
Schaller, G., Schaerer, D., Meynet, G., & Maeder, A. 1992, A&AS, 96, 269
Schmidt-Kaler, T. 1982, in Landolt Börnstein, Vol. I/2b, p. 15
Schrijver, C. J. 2002, AN, 323, 157
Schrijver, C. J., & Title, A. 2001, ApJ, 551, 1099
Soderblom, D., Jones, B. F., Balachandran, S., et al. 1993, AJ, 106, 1059
Strassmeier, K. G. 1996, A&A, 314, 558
Strassmeier, K. G. 2002, AN, 323, 309
Strassmeier, K. G., Boyd, L. J., Epand, D. H., & Granzer, T. 1997, PASP, 109, 697
Strassmeier, K. G., Granzer, T., Boyd, L. J., & Epand, D. 2000, Proc. SPIE, 4011, 157
Strassmeier, K. G., Kratzwald, L., & Weber, M. 2003, A&A, 408, 1103 (Paper XX)
Strassmeier, K. G., & Rice, J. B. 1998, A&A, 330, 685 (Paper VI)
Strassmeier, K. G., & Rice, J. B. 2003, A&A, 399, 315 (Paper XIX)
Strassmeier, K. G., Serkowitsch, E., & Granzer, T. 1999, A&AS, 140, 29
Strassmeier, K. G., Washuettl, A., Granzer, T., Scheck, M., & Weber, M. 2001, A&AS, 142, 275
Washuettl, A., & Strassmeier, K. G. 2001, A&A, 370, 218
Weber, M., & Strassmeier, K. G. 2001, A&A, 373, 974 (Paper XV)